Novel power-to-syngas concept for plasma catalytic reforming coupled with water electrolysis

Novel power-to-syngas concept for plasma catalytic reforming coupled with water electrolysis

Kai Li[§,a,c], Jing-Lin Liu[§,a,c], Xiao-Song Li[a,c], Hao-Yu Lian[a,c], Xiaobing Zhu[a,c,*], Annemie Bogaerts[b,*], Ai-Min Zhu[a,c,*]

[a]*Key Laboratory of Materials Modification by Laser, Ion and Electron Beams (Dalian University of Technology), Ministry of Education, Dalian 116024, China*
[b]*Research Group PLASMANT, Department of Chemistry, University of Antwerp, Universiteitsplein 1, BE-2610 Antwerp, Belgium*
[c]*Laboratory of Plasma Physical Chemistry, Center for Hydrogen Energy and Environmental Catalysis, Dalian University of Technology, Dalian 116024, China*

[§]*These authors contributed equally to this work.*
[*]*Corresponding authors. E-mail addresses: xzhu@dlut.edu.cn (X. Zhu); annemie.bogaerts@uantwerpen.be (A. Bogaerts); amzhu@dlut.edu.cn (A.M. Zhu)*

Abstract

We propose a novel Power to Synthesis Gas (P2SG) approach, composed of two high-efficiency and renewable electricity-driven units, i.e., plasma catalytic reforming (PCR) and water electrolysis (WE), to produce high-quality syngas from CH_4, CO_2 and H_2O. As WE technology is already commercial, we mainly focus on the PCR unit, consisting of gliding arc plasma and Ni-based catalyst, for oxidative dry reforming of methane. An energy efficiency of 78.9% and energy cost of 1.0 kWh/Nm^3 at a CH_4 conversion of 99% and a CO_2 conversion of 79% are obtained. Considering an energy efficiency of 80% for WE, the P2SG system yields an overall energy efficiency of 79.3% and energy cost of 1.8 kWh/Nm^3. High-quality syngas is produced without the need for post-treatment units, featuring the ideal stoichiometric number of 2, with concentration of 94.6 vol.%, and a desired CO_2 fraction of 1.9 vol.% for methanol synthesis. The PCR unit has the advantage of fast response to adapting to fluctuation of renewable electricity, avoiding local hot spots in the catalyst bed and coking, in contrast to conventional catalytic processes. Moreover, pure O_2 from the WE unit is directly utilized by the PCR unit for oxidative dry reforming of methane, and thus, no air separation unit, like in conventional processes, is required. This work demonstrates the viability of the P2SG approach for large-scale energy storage of renewable electricity via electricity-to-fuel conversion.

Keywords: Plasma catalysis; Plasma catalytic reforming; Power-to-syngas; Renewable energy

1. Introduction

Synthesis gas (syngas, H_2 + CO) is a crucial chemical feedstock for producing synthetic fuels and bulk chemicals via the Fischer-Tropsch (F-T) synthesis process[1, 2] and methanol synthesis process[3], which require a 2/1 molar ratio of H_2/CO. Methane is the preferred and main source for syngas generation, due to its plentiful supply (such as natural gas, shale gas and biogas) and its highest H/C atomic ratio. Three kinds of reforming reactions are generally used for syngas production from methane: steam reforming, carbon dioxide (dry) reforming and oxidative reforming (partial oxidation)[3-5].

Among the three reforming reactions, steam reforming and dry reforming have H_2/CO molar ratios of 3 and 1, respectively, which requires additional steps to adjust the H_2/CO ratios to 2. Although oxidative reforming theoretically has a H_2/CO ratio of 2, there exist technical issues of local hot spots, catalyst sintering and safety concerns in the catalytic process, besides expensive operating cost to obtain pure oxygen from air separation. Autothermal reforming (ATR), combining oxidative and steam reforming, normally produces a H_2/CO ratio higher than 2 and a considerable amount of CO_2 and H_2O in the product stream, which reduces the syngas purity, final product yield and total efficiency in the subsequent synthesis processes[3, 4, 6]. Indeed, the CO_2 and H_2O content of the syngas stream is another important factor relevant to the syngas quality.

Syngas with a H_2/CO ratio of 2 can be directly produced from the combination of steam and dry reforming of methane (called bi-reforming, abbreviated as BiRfm)[3, 4]:

$$3CH_4 + 2H_2O(g) + CO_2 \rightarrow 4CO + 8H_2 \qquad \Delta H^0_{298\,K} = 658.9\ \text{kJ/mol} \quad \text{(R1)}$$

However, the BiRfm reaction R1 consists of two strongly endothermic reactions, and is believed difficult and challenging, and excess steam and CO_2 are required to obtain higher methane conversion and to prevent carbon deposition on the catalysts[3, 4, 7, 8]. This inevitably leads to increasing the CO_2 and H_2O content in the syngas stream and thus it reduces the quality of the syngas stream.

Novel power-to-syngas (P2SG) approach

To solve the above-mentioned problem of BiRfm, in this paper we propose a novel combination of water splitting (R2) and oxidative dry reforming of methane (R3),

$$2H_2O(l) \rightarrow O_2 + 2H_2 \qquad \Delta H^0_{298\,K} = 571.6\ \text{kJ/mol} \quad \text{(R2)}$$

$$3CH_4 + O_2 + CO_2 \rightarrow 4CO + 6H_2 \qquad \Delta H^0_{298\,K} = 175.3\ \text{kJ/mol} \quad \text{(R3)}$$

The combination of reactions R2 and R3 gives a total reaction, R4,

$$3CH_4 + 2H_2O(l) + CO_2 \rightarrow 4CO + 8H_2 \qquad \Delta H^0_{298\,K} = 747\ \text{kJ/mol} \quad \text{(R4)}$$

Hence, it is reaction R1 plus a phase transfer process of water vaporization. As shown in figure 1, the standard enthalpy changes are 572 and 175 kJ/mol for reactions R2 and R3, respectively[9]. Thus, in terms of enthalpy change, reaction R2 accounts for the majority of the total reaction R4 (747 kJ/mol). It is clear that reaction R2 can be conducted easily and efficiently via water electrolysis (WE)[10]. A typical commercial electrolyzer has an efficiency of 80% and a higher efficiency can be obtained with elevated water temperature or steam[11, 12].

Moreover, pure O_2, as the side product of reaction R2, which evolves from the anode of the electrolyzer since the electrode compartments are separated, can

be directly utilized by reaction R3 without the need for separation. Hence, an air separation unit to obtain pure oxygen, as in conventional processes, is not needed.

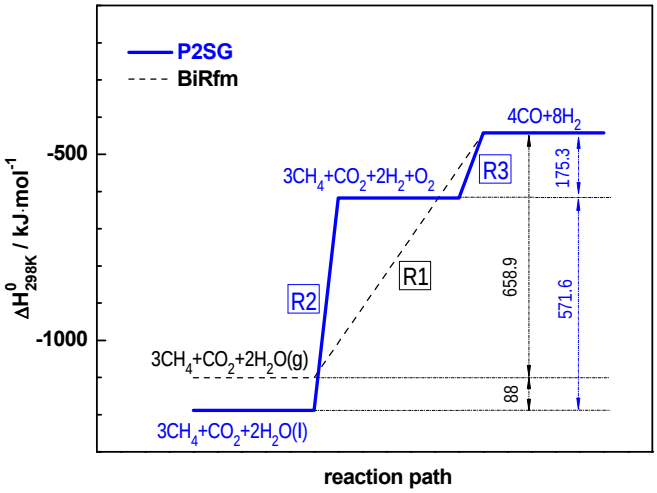

Figure 1. Standard enthalpy changes of high-quality syngas production from CH_4, H_2O and CO_2 in a 3/2/1 molar ratio, via reactions R2 and R3 of the P2SG approach, and via reaction R1 of the bi-reforming (BiRfm) approach.

In reaction R3, the combination of exothermic partial oxidation and endothermic dry reforming makes it weakly endothermic (175 kJ/mol). However, the conventional catalytic process bears a drawback of local hot spots, because the exothermic oxidation reaction proceeds rapidly in oxidizing atmosphere (near the catalyst-bed inlet), which results in catalyst sintering and subsequent deactivation[13, 14]. Ni-based catalysts are commonly employed and their deactivation is caused by the changes in valence state of the Ni active phase and carbon deposition, besides the above-mentioned sintering. To avoid these issues, we employ here plasma catalytic reforming (PCR)[15-20] for R3, where

oxidative reforming occurs in the plasma zone with complete consumption of oxygen.

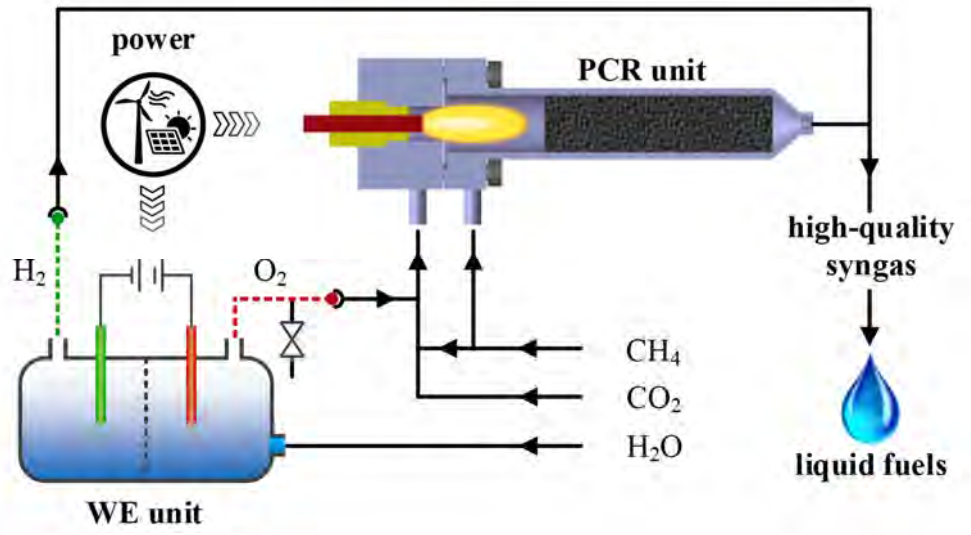

Figure 2. Schematic diagram of power to high-quality syngas via the new P2SG approach, which consists of a PCR unit and a WE unit, both driven by renewable electricity.

The two units of WE (for R2) and PCR (for R3), each of which can be driven by renewable electricity, are combined to produce high-quality syngas for subsequent downstream synthetic fuel production, so the overall concept is named power-to-syngas, P2SG. Figure 2 shows a schematic diagram of the P2SG approach. A detailed diagram of the PCR unit is presented in the Methods section. H_2O is split into pure H_2 and pure O_2, which evolve from the cathode and anode of the WE unit, respectively. Pure O_2 is utilized by reaction R3 in the PCR unit, and thus, no air separation unit, normally required for reaction R3, is needed here. In addition, pure H_2 is supplied to the product gas of reaction R3, hence to achieve high-quality syngas. The P2SG strategy is an attractive route to convert renewable, fluctuating electricity into chemical energy, stored on a large scale in synthetic fuels, due to its advantages of fast response and instant

adjustability, especially for the PCR unit[20], in contrast to conventional catalytic processes. Meanwhile, this strategy recycles the most serious greenhouse gas CO_2 as a feedstock, which can make an additional important contribution to mitigate the global CO_2 emission.

2. Experimental

For the P2SG approach, a new PCR reactor for oxidative dry reforming of methane is specially designed. A schematic diagram of the PCR reactor is shown in figure 3. A stainless-steel cylinder with inner diameter of 20 mm and length of 24 cm is grounded. The high-voltage electrode is electrically insulated by ceramic and located at the axis of the cylinder. A 5 kHz alternating current (AC) high-voltage power source is connected to the high-voltage electrode, to generate a gliding arc discharge (plasma zone in figure 3) at atmospheric pressure. The inlet gas flow $\boldsymbol{F_1}$ is tangential, creating a vortex flow in the plasma. The input plasma power is measured by a watt-meter installed at the transformer primary side of the power source.

The $Ni/CeO_2/Al_2O_3$ catalysts (see SI for details), containing Ni of 11 wt.% and Ce of 8 wt.%, are packed in the post-plasma zone, at a distance varying between 4.0 and 10.5 cm between plasma and catalyst. A home-made heater with a height of 20 cm, wrapped by ceramic fiber cotton on the outside of the heater for heat insulation, is employed for additional heating of the catalyst bed, needed due to the addition of $\boldsymbol{F_2}$ after the plasma. The axial distributions of the catalyst bed (T_{CB}) and reactor wall (T_{RW}) temperatures are measured by two movable thermocouples. The temperature of the heater, T_H, is controlled by the third thermocouple, fixed at the half-height of the heater. The power consumed by the

heater is measured by a PowerBay (Shenzhen Northmeter Co., China) and time-averaged over five hours.

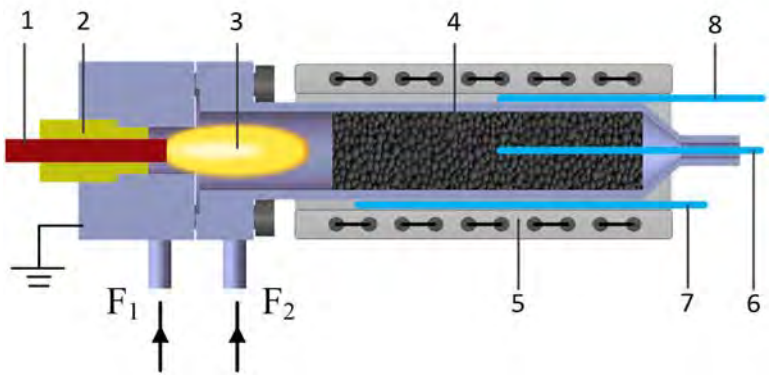

Figure 3. Schematic diagram of the plasma catalytic reactor. The numbers 1, 2, 3, 4, 5, 6, 7, 8, represent the high-voltage electrode, ceramic insulator, plasma zone, catalyst bed zone, heater, two movable thermocouples for recording the temperature of the catalyst bed and the reactor wall (6 for T_{CB} and 7 for T_{RW}), and a static thermocouple (8 for T_H) located at the half-height of the heater. The inlet gas flows $\boldsymbol{F_1}$ and $\boldsymbol{F_2}$ are fed into the reactor before and after the plasma, respectively.

To avoid coke formation and achieve complete O_2 consumption in the plasma, we use two separate inlet flows: the inlet flow $\boldsymbol{F_1}$ (3.0 SLM) with $CH_4/CO_2/O_2$ molar ratio of 3/2/2 is introduced before the plasma, while $\boldsymbol{F_2}$ (1.3 or 0.9 SLM) with pure CH_4 is introduced after the plasma. The $CH_4/CO_2/O_2$ molar ratios in the total flow $\boldsymbol{F_t}$ (4.3 or 3.9 SLM, i.e., $\boldsymbol{F_1}+\boldsymbol{F_2}$) are 3/1/1 (stoichiometric ratio of R3) or 2.5/1/1 (slight shortage of CH_4). The gas flow rates are controlled by mass flow controllers (Beijing Sevenstar Electronics Co., China). The specific energy input (*SEI*) in the plasma is calculated by the plasma input power divided by the flow rate $\boldsymbol{F_1}$. The gas hourly space velocity (GHSV) of the catalyst is obtained by the total flow rate $\boldsymbol{F_t}$ divided by the catalyst weight.

The thermodynamic-equilibrium (TE) conversions and concentrations as a function of the end temperature of the catalyst bed are calculated by the HSC Chemistry software (v7.0) using the Gibbs free energy minimization method; see more details in the SI.

Two gas chromatographs (Agilent 1790 T and Agilent 6890N) are employed for on-line analysis of the gaseous products using an internal standard method, which was described previously[21, 22]. N_2 and He are used as internal standard gases for quantification of O_2, CH_4, CO_2 and CO, and for quantification of H_2, respectively. The internal standard gases are mixed with the product stream at the outlet of the PCR reactor, they pass through a cold trap and are analyzed on-line by the two gas chromatographs. The definitions of conversion, carbon-based (C-based) selectivity and hydrogen-based (H-based) selectivity are listed in the SI.

3. Results

In the present work, reaction R3 in the PCR unit is crucial to the P2SG approach, and thus we focus here on this reaction. Reaction R2, occurring in the WE unit, is included in the Discussion section below. For the PCR unit, we first demonstrate the essential contribution of the gliding arc plasma (see Methods) in the oxidative dry reforming reaction.

3.1 Crucial role of the plasma

A flow of $CH_4/CO_2/O_2$ with molar ratio of 3/2/2 and flow rate of 3.0 SLM in vortex flow is introduced into the plasma at a specific energy input (*SEI*) of 27 kJ/mol. The arc, as shown in the inset of figure 4, is pushed and elongated by the vortex flow to rotate and glide with high velocity, which provides a highly active plasma region. As shown in figure S1, optical emission spectra of OH (*A*-*X*), CH

(*A*-*X*), C_2 (*A*-*X*), CO (*B*-*A*), H_α, H_β and O (3*p*-3*s*, 777 nm) are observed from the plasma in the wavelength range of 300-800 nm. The local (arc channel) gas temperature in the plasma cannot be measured directly, but can be estimated by the CO (*B*-*A*) rotational temperature of 2500 K (figure S2). The plasma has a high electron density of 2.7×10^{14} cm^{-3} (figure S3), and in combination with the high gas temperature of 2500 K in the arc channel (figure S2), it features high reaction rates. Therefore, O_2 is completely consumed in the plasma, which is indeed highly desired, to avoid catalyst sintering and deactivation in the subsequent catalytic stage (cf. previous section), and 64.8% of CH_4 is converted (figure 4a). The CO_2 conversion of -3.9% means that there is no net conversion for CO_2, because it is counteracted by complete oxidation of CH_4 producing some CO_2. From CH_4, 42.6% of the H atoms are converted to H_2, 2.9% to C_2 hydrocarbons and 55.0% to H_2O. The CO selectivity is 91.6% and a small amount of C_2 hydrocarbons is formed with 6.3% selectivity. A syngas concentration of 38.7 vol.% and H_2/CO ratio of 1.0 are obtained (figure 4b). The carbon balance is 97.9%, being close to 100%. Based upon the results of the conversions (64.8% of CH_4, 100% of O_2 and -3.9% of CO_2) and selectivities (42.6% of H_2 and 55.0% of H_2O), we can conclude that CH_4 is mainly converted in the plasma via reaction R5 and R6 with an approximately equivalent reaction rate,

$$CH_4 + 1/2O_2 \rightarrow CO + 2H_2 \quad \text{(R5)}$$

$$CH_4 + O_2 \rightarrow CO + 2H_2O \quad \text{(R6)}$$

The gliding arc plasma is integrated in the PCR unit (see figure 2 and Methods), and accounts already for a significant fraction of the CH_4 conversion, as well as an excellent energy efficiency, due to the non-equilibrium character of the plasma[20], besides complete O_2 consumption to avoid local hot spots and

catalyst sintering, as mentioned above. Unless otherwise specified, the PCR unit is conducted at a total flow rate $\boldsymbol{F_t}$ of 4.3 SLM $CH_4/CO_2/O_2$ with molar ratio of 3/1/1. More specifically, besides introducing 3.0 SLM flow rate into the plasma ($\boldsymbol{F_1}$), 1.3 SLM $\boldsymbol{F_2}$ of pure CH_4 is added after the plasma to obtain the $CH_4/CO_2/O_2$ ratio of 3/1/1 in $\boldsymbol{F_t}$, as this can avoid coking issues in the plasma. Furthermore, 41.0 g $Ni/CeO_2/Al_2O_3$ catalyst is placed after the active plasma region, with an additional heater. Indeed, the heating by the plasma is not sufficient due to the addition of CH_4 after the plasma (see figure 3 in Experimental).

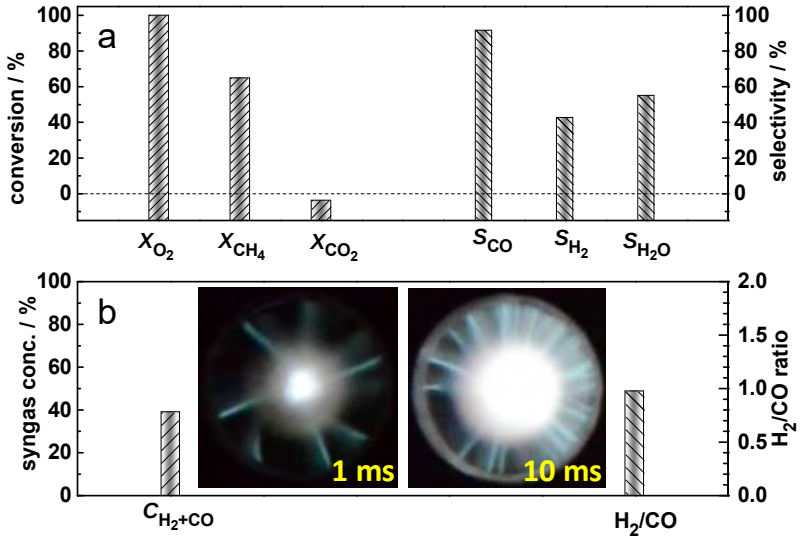

Figure 4. (a) O_2, CH_4 and CO_2 conversions, CO, H_2 and H_2O selectivities and (b) syngas concentration and H_2/CO ratio in the plasma, at a flow rate of 3.0 SLM with $CH_4/CO_2/O_2$ ratio of 3/2/2 and a *SEI* of 27 kJ/mol. Inset: plasma images in front view, at exposure times of 1 ms and 10 ms, showing the rotation of the arc.

As we reach an O_2 conversion of 100% for all PCR conditions investigated, in the following text we will only focus on the CH_4 and CO_2 conversions, selectivities, syngas concentration and H_2/CO ratio, as well as on the energy cost

and energy efficiency of the process. We will also compare with the obtained conversions and syngas concentrations by thermodynamic equilibrium (TE) calculations, as explained in the SI (figure S4).

3.2 Effect of the catalyst bed temperature

Figure 5 shows the axial temperature profiles of the catalyst bed, T_{CB}, for different temperatures of the heater, i.e., T_H of 1123, 1073, 1023, and 973 K, at a gas hourly space velocity (GHSV) of 6300 $mL \cdot g^{-1} \cdot h^{-1}$. Interestingly, the first 2 cm of the catalyst bed are characterized by a remarkable drop in T_{CB} at each T_H, with an almost identical curve independent of T_H. The remarkable drop in T_{CB} can be ascribed to the fact that large amounts of CH_4 are rapidly converted by the strongly endothermic reforming reaction, due to substantial heat and active species derived from the plasma. Specifically, T_{CB} drops from 1143-1163 K at the beginning to ~1013 K (with a slope of ~140 K/cm) within the first 1 cm, and to ~963 K (at a slope of ~50 K/cm) within the next 1 cm. After a further (minor) drop, it starts (slightly) rising again and approaches the temperature of the reactor wall (T_{RW}) at the end of the catalyst bed, as shown in figure S5.

Due to a great difference in temperature along the catalyst bed, we decided to use the end temperature of the catalyst bed (end T_{CB}) for the thermodynamic equilibrium (T_E) calculations (see SI). Consistent with the TE calculations, we also adopt the end T_{CB} for the experimental results versus temperature. The end T_{CB} rises slightly more than linearly upon increasing the heater temperature (T_H) from 973 to 1123 K, as shown in figure 6. It is slightly lower than T_H at e.g. 973 and 1023 K, while it is more or less equal to T_H at 1123 K. Accordingly, the CH_4

and CO_2 conversions increase remarkably from 69.2% and 45.5% to 92.1% and 85.1%, respectively, upon rising end T_{CB} from 948 to 1126 K; see figure 7a.

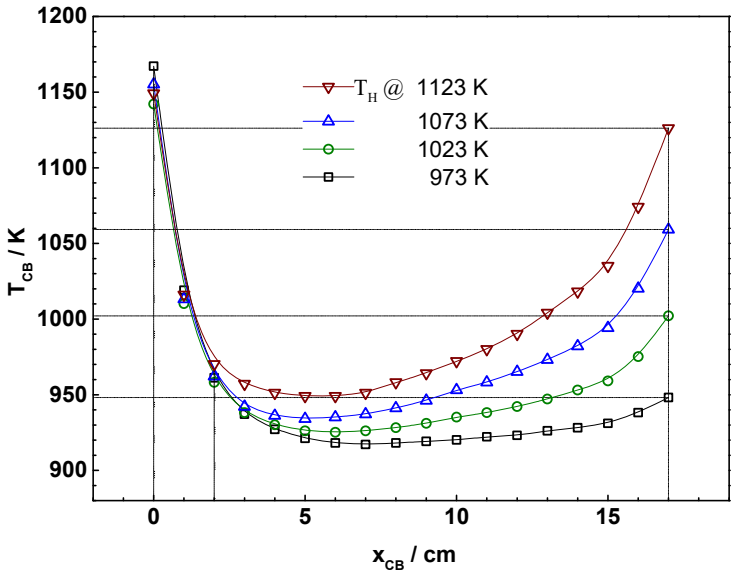

Figure 5. Axial profiles of T_{CB} at different T_H. $\boldsymbol{x_{CB}}$ is the axial distance from the entry of the catalyst bed. Conditions: a total flow rate of 4.3 SLM with $CH_4/CO_2/O_2$ ratio of 3/1/1, a *SEI* of 27 kJ/mol and a GHSV of 6300 $mL \cdot g^{-1} \cdot h^{-1}$.

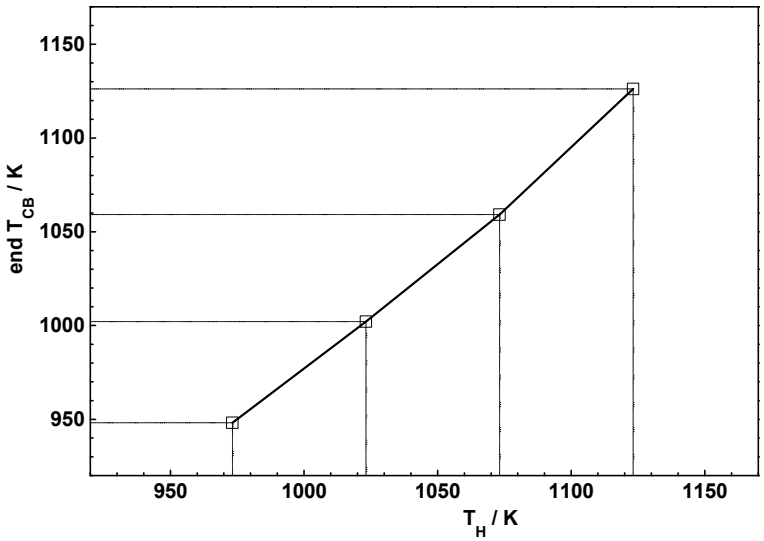

Figure 6. Dependence of end T_{CB} on T_H. The conditions are the same as in figure 5.

Note that the conversion in the first 2 cm of the catalyst bed, characterized by the fastest drop in T_{CB}, is mainly due to the heat and active species provided by the plasma, while further downstream, the additional catalyst bed heating accounts for the further catalytic conversion. The conversion of CH_4 is higher than CO_2, which is mainly ascribed to the side reaction of methane combustion[23]. Furthermore, it is consistent with other papers for plasma-based CO_2 and CH_4 conversion[24], and can be explained by model calculations[25, 26] because of the easier dissociation of CH_4 compared to CO_2.

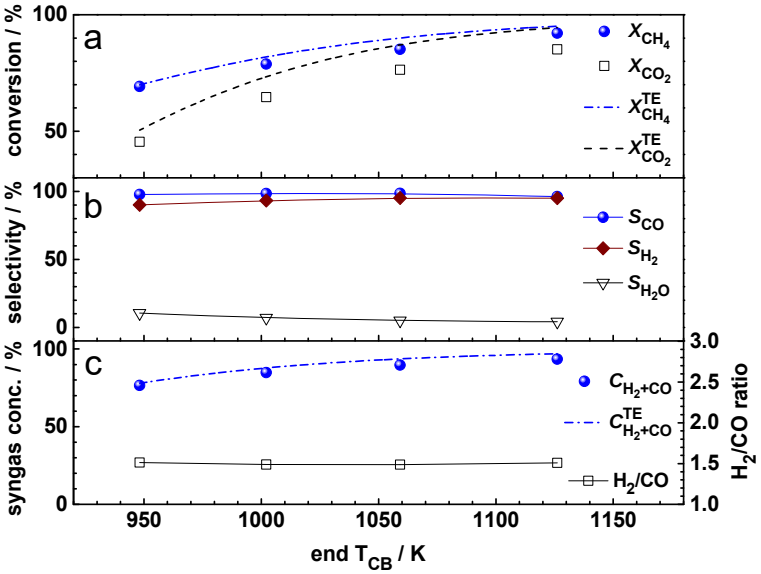

Figure 7. Effect of end T_{CB} (i.e., the end temperature of the catalyst bed) on (a) CH_4 and CO_2 conversion, (b) CO, H_2 and H_2O selectivity and (c) syngas concentration and H_2/CO ratio, at the same conditions as in figure 5. Comparison is also made with the corresponding values obtained from thermodynamic equilibrium (TE) calculations (see SI).

Figure 7b shows that the H_2 selectivity increases slightly from 90.1% to 95.1%, while the H_2O selectivity decreases accordingly from 10.5% to 4.1%, and

the CO selectivity remains constant at nearly 100% (see formulas used for these selectivities in the SI). In addition, the H_2/CO ratio also remains 1.5 (figure 7c), identical to the stoichiometric ratio in reaction R3, while the syngas concentration increases remarkably from 76.5 vol.% to 93.5 vol.%. Finally, when comparing with the TE calculations (see details in SI), it is clear that the experimental CH_4 conversion in figure 7a and the syngas concentration in figure 7c are very close to the TE values, while the CO_2 conversion is slightly lower; see figure 7a.

3.3 Effect of gas hourly space velocity (GHSV)

At T_H of 1123 K (end T_{CB} of 1126 K), the conversions of CH_4 (92.1%) and CO_2 (85.1%) are very high, so changing the GHSV will not have great effect on these conversions anymore. Therefore, we selected T_H at 1073 K to show the effect of GHSV on conversion, selectivity, syngas concentration and H_2/CO ratio; see figure 8. The GHSV is calculated as the total gas flow rate divided by the catalyst weight, so we have varied the amount of catalyst in figure 8 (from 41.0 g to 10.0 g), at a fixed total flow rate of 4.3 SLM. The effect on the end T_{CB} is also plotted (figure 8a).

The T_{CB} drops with the same slope in the first 2 cm of the catalyst bed at various GHSV, as shown in figure S6. The starting T_{CB} at a GHSV of 6300 $mL \cdot g^{-1} \cdot h^{-1}$ is higher than at a GHSV of 25700 $mL \cdot g^{-1} \cdot h^{-1}$ (i.e., 1155 K *vs* 1101 K), which is caused by a shorter distance between the plasma and the catalyst for the lower GHSV (corresponding to a larger amount of catalyst). Indeed, the distance between the plasma and the catalyst bed is 4.0 cm for the first case, and 10.5 cm for the latter case.

With a drop in GHSV from 25700 to 6300 mL·g^{-1}·h^{-1}, the end T_{CB} rises from 945 to 1059 K (see figure 8a and figure S6). As a result, the CH_4 and CO_2 conversions increase remarkably from 63.5% and 39.6% to 85.2% and 76.4%, respectively (figure 8a). Moreover, the H_2 selectivity increases from 87.5% to 95.2%, while the H_2O selectivity decreases accordingly, and the CO selectivity remains constant at approximately 100% (figure 8b). Furthermore, the H_2/CO ratio keeps constant at around 1.5, and a remarkable increase in syngas concentration from 70.9 vol.% to 89.7 vol.% is observed (figure 8c). In general, the CH_4 conversion and syngas concentration are again closer to the TE values than the CO_2 conversion (cf. figures 8a and 8c), which is consistent with the results in figures 7a and 7c.

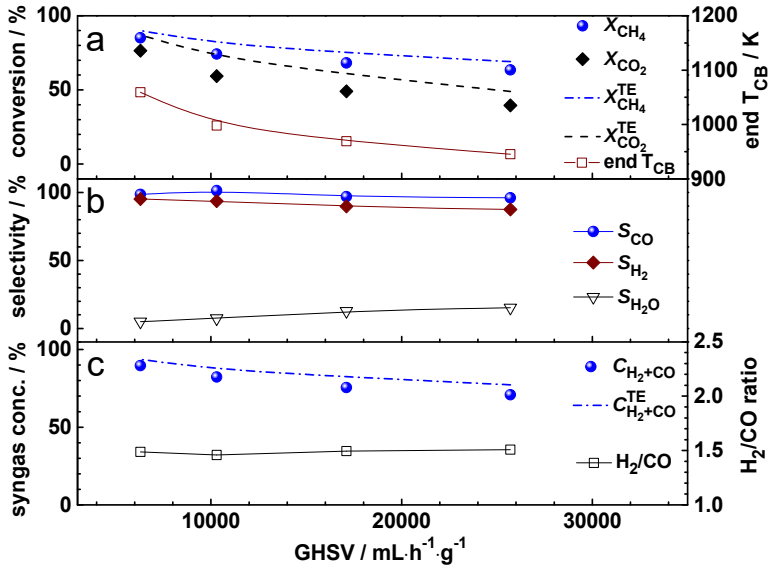

Figure 8. Effect of GHSV on (a) CH_4 and CO_2 conversion and end T_{CB}, (b) CO, H_2 and H_2O selectivity, and (c) syngas concentration and H_2/CO ratio, at T_H of 1073 K and a total flow rate of 4.3 SLM. Comparison is also made with the corresponding values obtained from thermodynamic equilibrium (TE) calculations (see SI).

3.4 Effect of $CH_4/CO_2/O_2$ ratio

It is worth noting that, for a conventional gas to liquid fuel system, the cost of reforming and post-treatment to produce sufficiently pure syngas accounts for above 50% of the total process cost[6, 27]. Indeed, the post-treatment incorporates a costly unit of water gas shift (WGS)[28, 29] reaction to adjust the H_2/CO ratio and an additional unit for separation of CH_4 and the excessive CO_2, to attain the needs for the downstream synthesis of fuels. Moreover, a certain amount of CO_2 (~2 vol%) needs to remain in the syngas for the downstream synthesis processes[30, 31] . Therefore, we should target these two aspects, i.e., a further improvement of the CH_4 conversion to ~100% and a remaining fraction of the appropriate amount of CO_2 (~2 vol%) in high-quality syngas. Hence, we will now investigate whether we can achieve this by tuning the $CH_4/CO_2/O_2$ ratio from 3/1/1 (stoichiometric ratio; cf. reaction R3 above) down to 2.5/1/1 (slight shortage of CH_4).

Figure 9 shows the effect of $CH_4/CO_2/O_2$ molar ratio on the conversions, selectivities, syngas concentration and H_2/CO ratio, by means of a variation in $\boldsymbol{F_2}$, and thus in $\boldsymbol{F_t}$ (keeping the same $\boldsymbol{F_1}$ of 3.0 SLM). The influence on the temperature profiles of the catalyst bed and reactor wall is presented in figure S7. Tuning the $CH_4/CO_2/O_2$ ratio down to 2.5/1/1 from the stoichiometric ratio 3/1/1 (of reaction R3), we can achieve a CH_4 conversion of 99.2%, thus nearly reaching 99.4% of the TE conversion (see figure 9a). This is because the CH_4 fraction is below stoichiometric and because of the slightly lower GHSV and thus slightly higher end T_{CB} (1153 K vs 1123 K; cf. figure S7). The CO_2 conversion slightly decreases to 79.4%, but also approaches the thermodynamic equilibrium conversion of 81.1%. The CO selectivity is nearly 100%, like before. The H_2 selectivity slightly decreases to 93.1%, with a slight increase in H_2O selectivity

to 7.2% (figure 9b). The syngas concentration remains at around 93 vol.%, and the H_2/CO ratio slightly decreases from 1.5 to 1.4 (figure 9c). As shown in figure S7, the temperature profiles of the reactor wall (T_{RW}) are very similar at $CH_4/CO_2/O_2$ molar ratios of 3/1/1 and 2.5/1/1, while the T_{CB} profile is slightly higher in the second half of the catalyst bed in case of $CH_4/CO_2/O_2$ molar ratio of 2.5/1/1, because of less remaining (unreacted) CH_4.

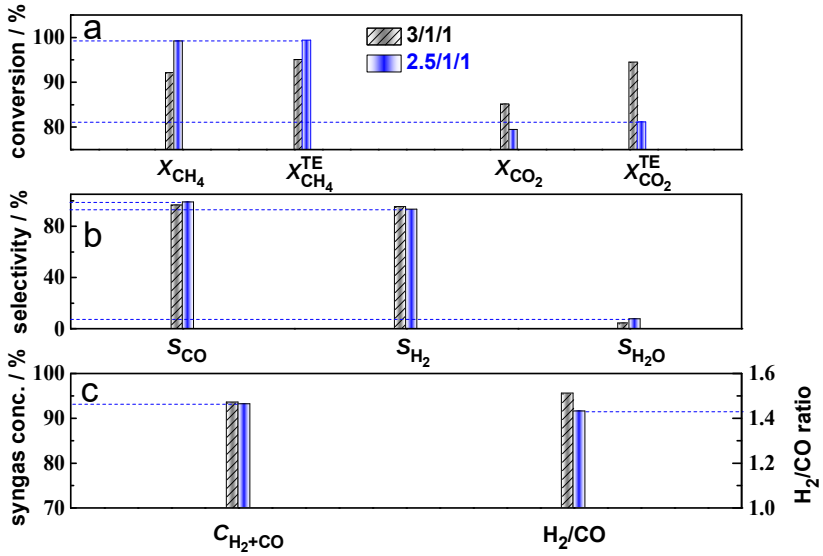

Figure 9. Effect of $CH_4/CO_2/O_2$ molar ratio on (a) CH_4 and CO_2 conversion, (b) CO, H_2 and H_2O selectivity, and (c) syngas concentration and H_2/CO ratio, at T_H of 1123 K. The GHSV for $CH_4/CO_2/O_2$ molar ratio of 3/1/1 and 2.5/1/1 is 6300 and 5700 $mL \cdot g^{-1} \cdot h^{-1}$, respectively, for the same amount of catalyst, to keep the same distance between plasma and catalyst (see details in SI). For the $CH_4/CO_2/O_2$ molar ratio of 2.5/1/1, the CH_4 flow rate after plasma ($\boldsymbol{F_2}$) is set at 0.9 SLM and the total flow rate ($\boldsymbol{F_t}$) is 3.9 SLM, while for the $CH_4/CO_2/O_2$ molar ratio of 3/1/1, the CH_4 flow rate after plasma ($\boldsymbol{F_2}$) and the total flow rate ($\boldsymbol{F_t}$) are set at 1.3 and 4.3 SLM, respectively (as before). Comparison is also made with the CH_4 and CO_2 conversions obtained from thermodynamic equilibrium (TE) calculations (see SI). The effect of $CH_4/CO_2/O_2$ molar ratio on the axial profiles of T_{CB} and T_{RW} is shown in figure S7.

3.5 Stability test and carbon balance

Figure S8 shows the stability of the conversions, syngas concentration and H_2/CO ratio, by plotting these values as a function of time-on-stream (TOS), i.e., operation time, for 5 hours, at T_H of 1123 K, GHSV of 5700 $mL \cdot g^{-1} \cdot h^{-1}$ and $CH_4/CO_2/O_2$ molar ratio of 2.5/1/1 (0.9 SLM $\boldsymbol{F_2}$ and 3.9 SLM $\boldsymbol{F_t}$). The CH_4 and CO_2 conversions stay constant at 99% and 79%, respectively, for a TOS of 5 h. The same applies for the flow rate of the PCR outlet gas (F_{out}^{PCR}), the syngas concentration and the H_2/CO ratio, which remain constant at 7.2 SLM, 93 vol.% and 1.4, respectively.

Interestingly, in contrast to the severe issue of coke formation by the conventional catalytic approach of BiRfm[3, 4], in our experiments coking is almost absent (see SI: figure S9) and accounts for only 0.08% of the total carbon input, as calculated from figure S10 and summarized in Table S1 of the SI. This value is negligible and much less than the 0.5% carbon deposition of shale gas to syngas conversion by the chemical looping approach[6]. This tiny amount of coke formation on the used catalyst (0.08% of the total carbon input) is in quite good accordance with the carbon balance between the inlet gas and outlet gas (40.2 mol *vs* 39.7 mol; cf. Table S1).

The almost absent coking in the P2SG approach can be attributed to two reasons: (1) a significant fraction of the CH_4 is converted in the plasma and thus the CH_4 concentration introduced into the catalyst bed is relatively low; (2) substantial active species derived from the plasma prevent the side reaction of coke formation on the catalysts. Hence, coke formation will not be a problem for the P2SG approach, which assures continuous running of the process to achieve high-quality syngas. In a chemical looping process, to suppress coke formation,

a small amount of O_2 is co-fed with $CH_4/CO_2/O_2$ ratio of 1/1/0.2, and thus the H_2/CO ratio (~ 1) is relatively low [32].

4. Discussion

So far, we have evaluated the PCR unit in terms of the added value of plasma (figure 4 and S1-S3), and the effect of catalyst bed temperature (figures 5-7 and S5), GHSV (figure 8 and S6), and $CH_4/CO_2/O_2$ molar ratio (figure 9 and S7) on the CH_4 and CO_2 conversion, product selectivities, syngas ratio and concentration, as well as on the stability and carbon balance (figures S8-S10, Table S1). Coupled with a WE unit, the PCR unit forms the novel P2SG system. Hence, we will now discuss the energy efficiency, energy cost, and syngas quality, for the separate PCR unit and for the entire P2SG system.

For the PCR unit, the CH_4 and CO_2 conversions are 99% and 79%, constant in time for at least 5 hours (cf. stability test in figure S8), at an optimal $CH_4/CO_2/O_2$ ratio of 2.5/1/1. The outlet gas of the PCR unit has a flow rate (F_{out}^{PCR}) of 7.2 SLM, and contains 54.8% H_2, 38.3% CO, 2.4% CO_2, 0.2% CH_4 and 4.3% H_2O in volume, as shown in Table 1. Furthermore, an energy efficiency η^{PCR} of 78.9% and an energy cost EC^{PCR} of 1.0 kWh/Nm^3 are obtained, according to equations E1, E2[18],

$$\eta^{PCR} = \frac{F_{out}^{PCR}(C_{H_2}^{PCR} \cdot LHV_{H_2} + C_{CO}^{PCR} \cdot HV_{CO})}{P^{PCR} + F_{CH_4}^{in} \cdot X_{CH_4} \cdot LHV_{CH_4}} \times 100\% \quad \text{(E1)}$$

$$EC^{PCR} = \frac{P^{PCR}}{F_{out}^{PCR}(C_{H_2}^{PCR} + C_{CO}^{PCR})} \quad \text{(E2)}$$

where LHV_{CH_4} and LHV_{H_2} denote the lower heating value of CH_4 and H_2, HV_{CO} is the heating value of CO, $F_{CH_4}^{in}$ is the inlet flow rate of CH_4, $C_{H_2}^{PCR}$ and C_{CO}^{PCR} are

the concentrations of H_2 and CO in the outlet gas, and P^{PCR} is the total power input in both the plasma and the heater of the PCR unit.

It should be noted that the temperature of the outlet gas (i.e., comparable to the end T_{CB}) is quite high (e.g., 1153 K at the most optimal conditions, cf. figure S7), and this heat could also further be utilized by a heat exchanger, to further improve the energy efficiency and reduce the energy cost[33]. This is not exploited in the present study, but will be done in our future work.

The presence of a low CO_2 concentration in syngas may promote the synthesis rate for the downstream fuel production[30, 31]. For instance, a CO_2 concentration of ~2 vol.%, as promoter for methanol synthesis[31], must be present in practice to achieve a high CO conversion into methanol. Hence, for methanol synthesis the ideal syngas stoichiometry is not a molar ratio H_2/CO of 2, but a molar ratio $(H_2-CO_2)/(CO+CO_2)$ of 2, also called the stoichiometric number (SN) of syngas[27]. The reverse water gas shift (RWGS) reaction explains why CO_2 appears in the SN. In the absence of CO_2, the SN is simplified as the molar ratio of H_2/CO.

The PCR unit in our study produces syngas with a SN of 1.3 (Table 1), which is less than the ideal value of 2. However, through H_2 addition from the WE unit, the ideal SN value of 2 can easily be reached in the P2SG system, as shown below and in Table 1.

Indeed, for the WE unit, the required H_2 flow rate, $F_{H_2}^{WE}$ to reach this ideal SN value of 2 is calculated in equation E3,

$$F_{H_2}^{WE} = F_{out}^{PCR}(2C_{CO}^{PCR} + 3C_{CO_2}^{PCR} - C_{H_2}^{PCR}) \quad \text{(E3)}$$

where $C_{CO_2}^{PCR}$ denotes the PCR outlet concentration of CO_2, and the other symbols were defined above. In this way, the required H_2 flow rate of the WE unit (cathode side) is calculated to be 2.1 SLM, yielding an oxygen flow rate of 1.05 SLM (at the anode side), of which 0.9 SLM O_2 is fed in the PCR unit and the rest may be vented.

Table 1. Flow rate and concentrations of the various products in the outlet gas, and the resulting $(H_2\text{-}CO_2)/(CO+CO_2)$ molar ratio (i.e., SN of syngas), as well as the input power, energy efficiency and energy cost, for the separate PCR and WE units, and the entire P2SG system. The results of the PCR unit are obtained at the same conditions as in figure S8. For the WE unit, the power and the energy cost are calculated with the assumption of an energy efficiency of 80%, and 2.1 SLM H_2 production rate, as required for the ideal SN value of 2 (see text).

unit	power / W	flow rate of outlet gas / SLM	concentration in outlet gas / vol.%					$(H_2\text{-}CO_2)/(CO+CO_2)$	energy efficiency	energy cost / $kWh \cdot Nm^{-3}$
			H_2	CO	CO_2	CH_4	H_2O			
PCR	397 [a]	7.2	54.8	38.3	2.4	0.2	4.3	1.3	78.9%	1.0
WE	560	2.1	100	/	/	/	/	/	80%[12]	4.4
P2SG	957	9.3	65.0	29.6	1.9	0.2	3.3	2.0	79.3%	1.8

[a] sum of input power for plasma and heater.

For the P2SG system, the mixture of 7.2 SLM outlet gas of the PCR unit and 2.1 SLM H_2 of the WE unit yields high-quality syngas of 9.3 SLM with the ideal SN of 2 (see Table 1). Furthermore, the syngas concentration (i.e., sum of H_2 and CO concentrations) increases from 93.1 vol.% in the PCR unit, to 94.6 vol.% in the P2SG system, and the CO_2 concentration of the P2SG system reaches a favorable 1.9 vol.%, which approaches the optimal CO_2 concentration of ~2 vol.%[31].

As mentioned above, the required H_2 flow rate of 2.1 SLM is obtained from liquid water via the WE unit, and it is mixed with the outlet gas of the PCR unit. Assuming an energy efficiency of the WE unit, η^{WE} of 80%[11, 12], the input power, P^{WE} and the energy cost of the WE unit, EC^{WE} are calculated according to equations E4 and E5,

$$P^{WE} = \frac{F_{H_2}^{WE} \cdot HHV_{H_2}}{\eta^{WE}} \tag{E4}$$

$$EC^{WE} = \frac{P^{WE}}{F_{H_2}^{WE}} \tag{E5}$$

where HHV_{H_2} denotes the higher heating value of H_2. The obtained values for the input power and energy cost of the WE unit are also listed in Table 1.

Finally, the energy efficiency, η^{P2SG} and energy cost, EC^{P2SG} of the entire P2SG system are calculated according to equations E6, E7,

$$\eta^{P2SG} = \frac{F_{out}^{P2SG}(C_{H_2}^{P2SG} \cdot LHV_{H_2} + F_{CO}^{P2SG} \cdot HV_{CO})}{P^{PCR} + P^{WE} + F_{CH_4}^{in} \cdot X_{CH_4} \cdot LHV_{CH_4}} \times 100\% \tag{E6}$$

$$EC^{P2SG} = \frac{P^{PCR} + P^{WE}}{F_{out}^{P2SG}(C_{H_2}^{P2SG} + C_{CO}^{P2SG})} \tag{E7}$$

where F_{out}^{P2SG} represents the P2SG outlet flow rate, and $C_{H_2}^{P2SG}$ and C_{CO}^{P2SG} are the P2SG outlet concentrations of H_2 and CO, respectively.

As a result, the P2SG system yields an energy efficiency of 79.3% and an energy cost of 1.8 kWh/Nm^3, and it produces 9.3 SLM high-quality syngas, with an ideal SN value of 2, nearly complete CH_4 conversion and a syngas concentration of 94.6 vol.%. Therefore, the P2SG system achieves high-quality

syngas and does not require expensive post-treatments, which distinguishes it from conventional syngas production processes.

5. Conclusions

We have developed a conceptually new approach of P2SG, composed of two high efficiency units, i.e., PCR and WE, both driven by renewable electricity, to efficiently produce high-quality syngas from CH_4, CO_2 and H_2O. The PCR unit performs oxidative dry reforming of methane, by means of pure O_2 produced from the anode of the WE unit. The H_2 produced from the cathode of the WE unit is added to the outlet gas of the PCR unit, yielding an SN value of 2 for the P2SG product gas, which is ideal for subsequent downstream synthetic fuel production.

To summarize, WE is used to produce pure H_2 added for the ideal SN of syngas, while pure O_2, as the side product of WE, is utilized simultaneously by the P2SG process for the oxidative dry reforming reaction. Therefore, no air separation unit, like in conventional processes, is required. This is one of the novelties of the P2SG process.

As WE technology is well developed and commercialized, our experimental investigation focuses mainly on the PCR unit, consisting of a gliding arc plasma and Ni-based catalyst. We demonstrate the added value of the plasma process, to account already for a significant fraction of the CH_4 conversion, as well as an excellent energy efficiency, due to the non-equilibrium character of the plasma[20], besides almost absent coking and complete O_2 consumption to avoid local hot spots in the catalyst bed. At optimized conditions of 3.9 SLM flow rate, with $CH_4/CO_2/O_2$ molar ratio of 2.5/1/1, a plasma *SEI* of 27 kJ/mol, a heater

temperature of 1123 K and a GHSV of 5700 $mL \cdot g^{-1} \cdot h^{-1}$, the PCR unit exhibits an energy efficiency of 78.9% and an energy cost of 1.0 kWh/Nm^3 at a CH_4 conversion of 99% and a CO_2 conversion of 79%.

Assuming an energy efficiency of 80% for the WE unit, we achieve an overall energy efficiency of 79.3% and an energy cost of 1.8 kWh/Nm^3 for the P2SG system. The high-quality syngas produced by the P2SG system features the ideal SN value of 2, a syngas concentration of 94.6 vol.%, and a desired CO_2 concentration of 1.9 vol.% for methanol synthesis. Therefore, the P2SG approach does not require expensive post-treatment, which distinguishes it from conventional syngas production processes. This work demonstrates the viability of the P2SG approach for large-scale energy storage of renewable electricity via electricity-to-fuel conversion. Indeed, there is no solid evidence yet that the combination with WE unit will effectively work, but this will be studied in the near future.

Acknowledgements

This project is supported by the National Natural Science Foundation of China (11705019, 11475041), the Fundamental Research Funds for the Central Universities (DUT16QY49, DUT16LK16) and the Fund for Scientific Research Flanders (FWO; grant G.0383.16N).

References

[1] F. Jiao, J. Li, X. Pan, J. Xiao, H. Li, H. Ma, M. Wei, Y. Pan, Z. Zhou, M. Li, S. Miao, J. Li, Y. Zhu, D. Xiao, T. He, J. Yang, F. Qi, Q. Fu, X. Bao, Selective conversion of syngas to light olefins, Science 351 (2016) 1065-1068.

[2] L. Zhong, F. Yu, Y. An, Y. Zhao, Y. Sun, Z. Li, T. Lin, Y. Lin, X. Qi, Y. Dai, L. Gu, J. Hu, S. Jin, Q. Shen, H. Wang, Cobalt carbide nanoprisms for direct production of lower olefins from syngas, Nature 538 (2016) 84.

[3] G.A. Olah, A. Goeppert, M. Czaun, G.K.S. Prakash, Bi-reforming of methane from any source with steam and carbon dioxide exclusively to metgas ($CO\text{-}2H_2$) for methanol and hydrocarbon synthesis, J. Am. Chem. Soc. 135 (2013) 648-650.

[4] G.A. Olah, A. Goeppert, M. Czaun, T. Mathew, R.B. May, G.K.S. Prakash, Single step bi-reforming and oxidative bi-reforming of methane (natural gas) with steam and carbon dioxide to metgas ($CO\text{-}2H_2$) for methanol synthesis: Self-sufficient effective and exclusive oxygenation of methane to methanol with oxygen, J. Am. Chem. Soc. 137 (2015) 8720-8729.

[5] F.J. Keil, Methane activation oxidation goes soft, Nat. Chem. 5 (2013) 91-92.

[6] S. Luo, L. Zeng, D. Xu, M. Kathe, E. Chung, N. Deshpande, L. Qin, A. Majumder, T.L. Hsieh, A. Tong, Z.C. Sun, L.S. Fan, Shale gas-to-syngas chemical looping process for stable shale gas conversion to high purity syngas with a H_2-CO ratio of 2, Energy Environ. Sci. 7 (2014) 4104-4117.

[7] M.M. Danilova, Z.A. Fedorova, V.I. Zaikovskii, A.V. Porsin, V.A. Kirillov, T.A. Krieger, Porous nickel-based catalysts for combined steam and carbon dioxide reforming of methane, Appl. Catal. B 147 (2014) 858-863.

[8] W.J. Jang, D.W. Jeong, J.O. Shim, H.M. Kim, H.S. Roh, I.H. Son, S.J. Lee, Combined steam and carbon dioxide reforming of methane and side reactions: Thermodynamic equilibrium analysis and experimental application, Appl. Energy 173 (2016) 80-91.

[9] D.R. Lide, CRC handbook of chemistry and physics, 90th ed., CRC Press/Taylor and Francis, Boca Raton, FL2009.

[10] C. Delacourt, P.L. Ridgway, J.B. Kerr, J. Newman, Design of an electrochemical cell making syngas ($CO+H_2$) from CO_2 and H_2O reduction at room temperature, J. Electrochem. Soc. 155 (2008) B42-B49.

[11] M. Gotz, J. Lefebvre, F. Mors, A.M. Koch, F. Graf, S. Bajohr, R. Reimert, T. Kolb, Renewable power-to-gas: A technological and economic review, Renewable Energy 85 (2016) 1371-1390.

[12] G.A. Olah, A. Goeppert, G.K.S. Prakash, Beyond oil and gas: The methanol economy, 2nd ed., Wiley-VCH: Weinheim2009.

[13] T.V. Choudhary, V.R. Choudhary, Energy-efficient syngas production through catalytic oxy-methane reforming reactions, Angew. Chem. Int. Edit. 47 (2008) 1828-1847.

[14] A.P.E. York, T.C. Xiao, M.L.H. Green, J.B. Claridge, Methane oxyforming for synthesis gas production, Catal. Rev. 49 (2007) 511-560.

[15] J.C. Whitehead, Plasma-catalysis: the known knowns, the known unknowns and the unknown unknowns, J. Phys. D 49 (2016).

[16] E.C. Neyts, K. Ostrikov, M.K. Sunkara, A. Bogaerts, Plasma catalysis: Synergistic effects at the nanoscale, Chem. Rev. 115 (2015) 13408-13446.

[17] K. Li, J.L. Liu, X.S. Li, X.B. Zhu, A.M. Zhu, Post-plasma catalytic oxidative CO_2 reforming of methane over Ni-based catalysts, Catal. Today 256 (2015) 96-101.

[18] K. Li, J.L. Liu, X.S. Li, X.B. Zhu, A.M. Zhu, Warm plasma catalytic reforming of biogas in a heat-insulated reactor: Dramatic energy efficiency and catalyst auto-reduction, Chem. Eng. J. 288 (2016) 671-679.

[19] W.C. Chung, M.B. Chang, Review of catalysis and plasma performance on dry reforming of CH_4 and possible synergistic effects, Renewable Sust. Energy Rev. 62 (2016) 13-31.

[20] R. Snoeckx, A. Bogaerts, Plasma technology - a novel solution for CO_2 conversion?, Chem. Soc. Rev. 46 (2017) 5805-5863.

[21] X.S. Li, B. Zhu, C. Shi, Y. Xu, A.M. Zhu, Carbon dioxide reforming of methane in kilohertz spark-discharge plasma at atmospheric pressure, AIChE J. 57 (2011) 2854-2860.

[22] B. Zhu, X.S. Li, J.L. Liu, X.B. Zhu, A.M. Zhu, Kinetics study on carbon dioxide reforming of methane in kilohertz spark-discharge plasma, Chem. Eng. J. 264 (2015) 445-452.

[23] A.G. Bhavani, W.Y. Kim, J.W. Lee, J.S. Lee, Influence of metal particle size on oxidative CO_2 reforming of methane over supported nickel catalysts: Effects of second-metal addition, ChemCatChem 7 (2015) 1445-1452.

[24] E. Cleiren, S. Heijkers, M. Ramakers, A. Bogaerts, Dry reforming of methane in a gliding arc plasmatron: Towards a better understanding of the plasma chemistry, ChemSusChem 10 (2017) 4025-4036.

[25] R. Snoeckx, Y.X. Zeng, X. Tu, A. Bogaerts, Plasma-based dry reforming: Improving the conversion and energy efficiency in a dielectric barrier discharge, RSC Adv. 5 (2015) 29799-29808.

[26] R. Snoeckx, R. Aerts, X. Tu, A. Bogaerts, Plasma-based dry reforming: A computational study ranging from the nanoseconds to seconds time scale, J. Phys. Chem. C 117 (2013) 4957-4970.

[27] J.P. Lange, Methanol synthesis: a short review of technology improvements, Catal. Today 64 (2001) 3-8.

[28] I. Wender, Reactions of synthesis gas, Fuel Process. Technol. 48 (1996) 189-297.

[29] P. Kang, Z.F. Chen, A. Nayak, S. Zhang, T.J. Meyer, Single catalyst electrocatalytic reduction of CO_2 in water to H_2+CO syngas mixtures with water oxidation to O_2, Energy Environ. Sci. 7 (2014) 4007-4012.

[30] J.J. Spivey, A. Egbebi, Heterogeneous catalytic synthesis of ethanol from biomass-derived syngas, Chem. Soc. Rev. 36 (2007) 1514-1528.

[31] K. Klier, V. Chatikavanij, R.G. Herman, G.W. Simmons, Catalytic synthesis of methanol from CO/H_2: 4. The effects of carbon dioxide, J. Catal. 74 (1982) 343-360.

[32] J. Hu, V.V. Galvita, H. Poelman, C. Detavernier, G.B. Marin, Catalyst-assisted chemical looping auto-thermal dry reforming: Spatial structuring effects on process efficiency, Appl. Catal. B 231 (2018) 123-36.
[33] C.S. Kalra, A.F. Gutsol, A.A. Fridman, Gliding arc discharges as a source of intermediate plasma for methane partial oxidation, IEEE Trans. Plasma Sci. 33 (2005) 32-41.

Supplementary information

Novel power-to-syngas concept for plasma catalytic reforming coupled with water electrolysis

Kai Li[§,a,c], *Jing-Lin Liu*[§,a,c], *Xiao-Song Li*[a,c], *Hao-Yu Lian*[a,c], *Xiaobing Zhu*[a,c,*], *Annemie Bogaerts*[b,*], *Ai-Min Zhu*[a,c,*]

[a]Key Laboratory of Materials Modification by Laser, Ion and Electron Beams (Dalian University of Technology), Ministry of Education, Dalian 116024, China

[b]Research Group PLASMANT, Department of Chemistry, University of Antwerp, Universiteitsplein 1, BE-2610 Antwerp, Belgium

[c]Laboratory of Plasma Physical Chemistry, Center for Hydrogen Energy and Environmental Catalysis, Dalian University of Technology, Dalian 116024, China

[§]These authors contributed equally to this work.

*Corresponding authors. E-mail addresses: xzhu@dlut.edu.cn (X. Zhu); annemie.bogaerts@uantwerpen.be (A. Bogaerts); amzhu@dlut.edu.cn (A. Zhu)

Contents

S1 Definitions and formulas

The definitions of conversion, carbon-based (C-based) and hydrogen-based (H-based) selectivity, carbon and hydrogen balances are as follows, consistent with our previous works [1-4]:

The conversion is defined as:

$$X_x(\%) = (\frac{F_x^{in} - F_x^{out}}{F_x^{in}}) \times 100 \quad \text{(SE1)}$$

where F_x^{in} and F_x^{out} are the inlet and outlet flow rate of reactant x. In the present work, the outlet flow rate of x (CH_4, O_2 or CO_2) is obtained by the flow rate (F_{N_2}) of the internal standard N_2 and the concentration ratio of x to N_2: $F_x^{out} = F_{N_2} \cdot \frac{C_x^{in}}{C_{N_2}^{out}}$. Thus, the conversions of CH_4 (X_{CH_4}), O_2 (X_{O_2}) and CO_2 (X_{CO_2}) are calculated as:

$$X_{CH_4} = (1 - \frac{F_{N_2}}{F_{CH_4}^{in}} \cdot \frac{C_{CH_4}^{out}}{C_{N_2}^{out}}) \times 100\% \quad \text{(SE2)}$$

$$X_{O_2} = (1 - \frac{F_{N_2}}{F_{O_2}^{in}} \cdot \frac{C_{O_2}^{out}}{C_{N_2}^{out}}) \times 100\% \quad \text{(SE3)}$$

$$X_{CO_2} = (1 - \frac{F_{N_2}}{F_{CO_2}^{in}} \cdot \frac{C_{CO_2}^{out}}{C_{N_2}^{out}}) \times 100\% \quad \text{(SE4)}$$

where $F_{CH_4}^{in}$, $F_{O_2}^{in}$ and $F_{CO_2}^{in}$ denote the flow rates of CH_4, O_2 and CO_2 fed into the reactor, respectively, and $C_{N_2}^{out}$, $C_{CH_4}^{out}$, $C_{O_2}^{out}$ and $C_{CO_2}^{out}$ represent the concentrations of N_2, CH_4, O_2 and CO_2 in the effluent gas, respectively.

The carbon-based (C-based) selectivity of CO (S_{CO}) is defined as:

$$S_{CO} = (\frac{F_{N_2}}{F_{CH_4}^{in} \cdot X_{CH_4} + F_{CO_2}^{in} \cdot X_{CO_2}} \cdot \frac{C_{CO}^{out}}{C_{N_2}^{out}}) \times 100\% \quad \text{(SE5)}$$

where C_{CO}^{out} denotes the concentration of CO in the effluent gas.

The hydrogen-based (H-based) selectivities of H_2 (S_{H_2}) and H_2O (S_{H_2O}) are defined as:

$$S_{H_2} = \frac{0.5 \cdot F_{He}}{F_{CH_4}^{in} \cdot X_{CH_4}} \cdot \frac{C_{H_2}^{out}}{C_{He}^{out}} \times 100\% \quad \text{(SE6)}$$

$$S_{H_2O} = \frac{0.5 \cdot F^{out}_{H_2O}}{F^{in}_{CH_4} \cdot X_{CH_4}} \times 100\% \quad \text{(SE7)}$$

where F_{He} denotes the flow rate of internal standard helium gas, $C^{out}_{H_2}$ and C^{out}_{He} represent the concentrations of H_2 and helium in the effluent gas, respectively; and $F^{out}_{H_2O}$ denotes the flow rate of H_2O produced, which can be calculated via SE8, assuming an oxygen balance of 100%,

$$F^{out}_{H_2O} = 2 \cdot (F^{in}_{CO_2} \cdot X_{CO_2} + F^{in}_{O_2} \cdot X_{O_2}) - F_{N_2} \cdot \frac{C^{out}_{CO}}{C^{out}_{N_2}} \quad \text{(SE8)}$$

The concentrations of syngas and carbon dioxide are:

$$C_{H_2+CO} = \frac{F_{N_2} \cdot \frac{C^{out}_{CO}}{C^{out}_{N_2}} + F_{He} \cdot \frac{C^{out}_{H_2}}{C^{out}_{He}}}{F_{N_2} \cdot (\frac{C^{out}_{CH_4}}{C^{out}_{N_2}} + \frac{C^{out}_{CO_2}}{C^{out}_{N_2}} + \frac{C^{out}_{O_2}}{C^{out}_{N_2}} + \frac{C^{out}_{CO}}{C^{out}_{N_2}} + \frac{C^{out}_{C_2}}{C^{out}_{N_2}}) + F_{He} \cdot \frac{C^{out}_{H_2}}{C^{out}_{He}} + F^{out}_{H_2O}} \times 100\% \quad \text{(SE9)}$$

$$C_{CO_2} = \frac{F_{N_2} \cdot \frac{C^{out}_{CO_2}}{C^{out}_{N_2}}}{F_{N_2} \cdot (\frac{C^{out}_{CH_4}}{C^{out}_{N_2}} + \frac{C^{out}_{CO_2}}{C^{out}_{N_2}} + \frac{C^{out}_{O_2}}{C^{out}_{N_2}} + \frac{C^{out}_{CO}}{C^{out}_{N_2}} + \frac{C^{out}_{C_2}}{C^{out}_{N_2}}) + F_{He} \cdot \frac{C^{out}_{H_2}}{C^{out}_{He}} + F^{out}_{H_2O}} \times 100\% \quad \text{(SE10)}$$

S2 Optical emission spectra (OES) diagnostics of the plasma

The gas temperature and electron density are two critical parameters for plasma chemical processes. From OES, these two parameters can be obtained. As shown in figure S1, at conditions of $CH_4/CO_2/O_2$=3/2/2, $\boldsymbol{F}_1$ flow rate of 3.0 SLM and *SEI* of 27 kJ/mol, emission spectra of OH (*A*-*X*), CH (*A*-*X*), C_2 (*A*-*X*), CO (*B*-*A*), H_α, H_β and O (3*p*-3*s*, 777 nm) are observed from the plasma in the wavelength range of 300-800 nm. Amongst them, the spectrum of CO can be used to determine the rotational temperature of CO, and the latter can be used as an estimate of the gas temperature in the plasma. The spectrum of H_β can be used to evaluate the electron density via its Stark broadening.

A rotational temperature of CO of 2500 K is obtained by fitting calculation, using a similar procedure as in our previous work[5], as shown in figure S2.

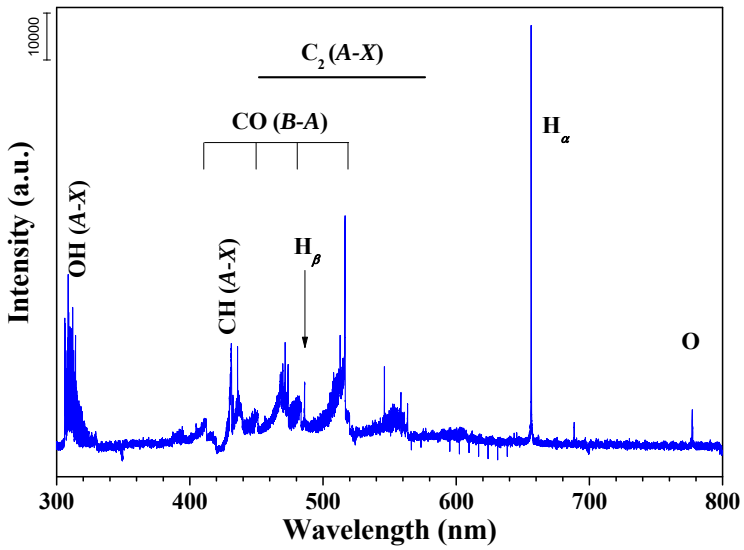

Figure S1. OES of the oxidative dry reforming of methane process in the plasma.

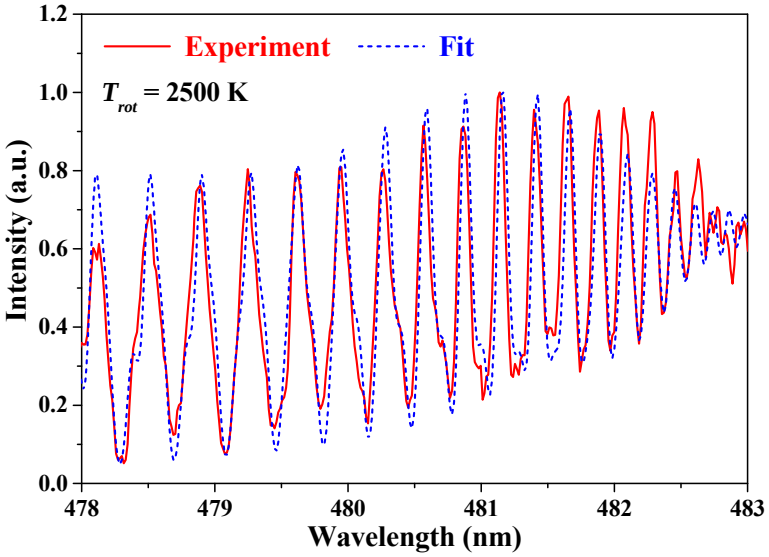

Figure S2. Experimental and fitted spectra of CO, to obtain the rotational temperature of CO.

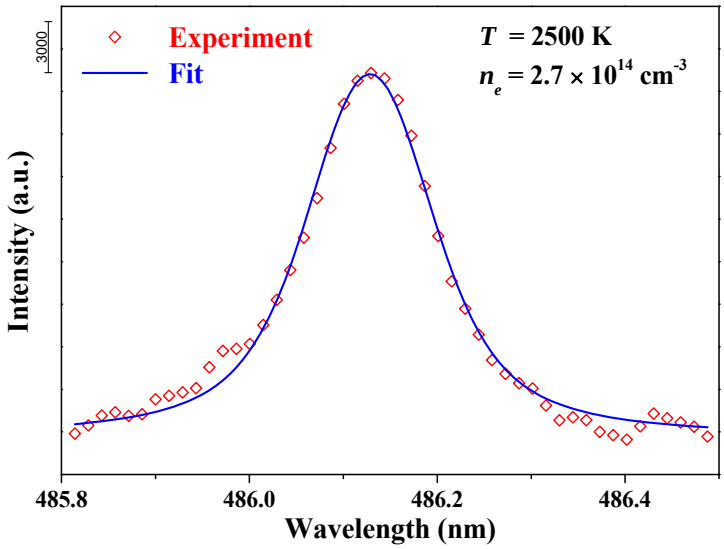

Figure S3. Voigt profile of the H_β line

The Hβ line shape in the plasma should be a Voigt profile, which is a convolution of Gaussian and Lorentz profiles. The Gaussian profile ($\Delta\lambda_{Gauss}$) is caused by instrumental and Doppler broadening. The Lorentz profile ($\Delta\lambda_{Lorentz}$) is induced by natural, resonance, van der Waals and Stark broadening.

$$\Delta\lambda_{Gauss} = \sqrt{\Delta\lambda_{instrumental}^2 + \Delta\lambda_{Doppler}^2} \quad \text{(SE11)}$$

$$\Delta\lambda_{Lorentz} = \Delta\lambda_{Natural} + \Delta\lambda_{\mathrm{Re}sonance} + \Delta\lambda_{van\ der\ waals} + \Delta\lambda_{Stark} \quad \text{(SE12)}$$

Since natural and resonance broadening are negligible compared with the other broadenings, the Stark broadening can be determined by a fitting profile of the Hβ line, based on instrumental, Doppler and van der Waals broadening. Subsequently, the electron density can be calculated via equation SE13 [6],

$$\Delta\lambda_{\mathrm{Stark}} = 2\times10^{-11} n_e^{2/3} \quad \text{(SE13)}$$

The electron density is evaluated as 2.7×10^{14} cm^{-3} at conditions of $CH_4/CO_2/O_2$=3/2/2, $\boldsymbol{F}_1$ flow rate of 3.0 SLM and *SEI* of 27 kJ/mol (see figure S3). Here, the instrumental broadening ($\Delta\lambda_{instrumental}$) is directly measured by a Hg-Ar lamp, which is 0.10 nm in this work. The Doppler ($\Delta\lambda_{Doppler}$) and van der Waals ($\Delta\lambda_{van\ der\ waals}$) broadenings are calculated via equation SE14 and SE15, respectively,

$$\Delta\lambda_{Doppler} = 7.16\times10^{-7}\lambda_0\sqrt{T/M} \quad \text{(SE14)}$$

$$\Delta\lambda_{van\ der\ waals} = 3.6p/T^{0.7} \quad \text{(SE15)}$$

where λ_0 is the wavelength (in nm); *T* is the gas temperature (K); M is the molar mass of a H atom (g/mol), and *p* is the pressure (in bar).

S3 Thermodynamic equilibrium (TE) calculation

Thermodynamic-equilibrium (TE) data was calculated by the HSC Chemistry software (v7.0) using the Gibbs free energy minimization method. The effect of temperature (in the range of 900-1200 K, at 1 bar) on the calculated TE conversions of CH_4, CO_2 and O_2 and the syngas concentration are shown in figure S4, for $CH_4/CO_2/O_2$ molar ratios of 3/1/1 (a) and 2.5/1/1 (b).

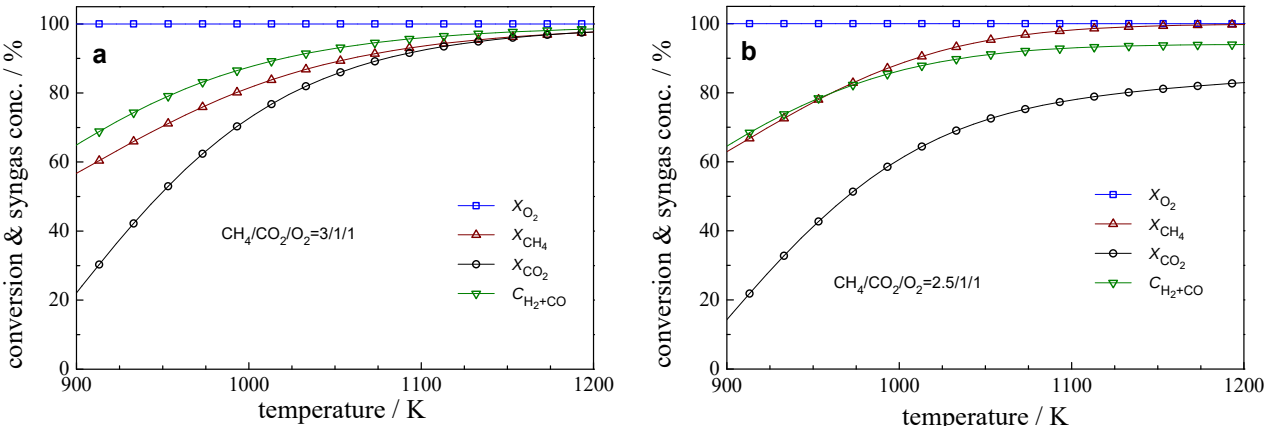

Figure S4. Effect of temperature on thermodynamic-equilibrium (TE) conversions and syngas concentration for $CH_4/CO_2/O_2$ molar ratios of (a) 3/1/1 and (b) 2.5/1/1 at 1 bar.

S4 Catalyst preparation and temperature distributions of catalyst bed and reactor wall

The $Ni/CeO_2/Al_2O_3$ catalysts are prepared by the sequential incipient wetness impregnation method using γ-Al_2O_3 pellets (ca. 2 mm diameter) as the supports. The support is impregnated overnight at room temperature with $Ce(NO_3)_3{\cdot}6H_2O$ solution, dried at 110 °C for 6 h and calcined in air at 500 °C for 6 h. Then the obtained CeO_2/Al_2O_3 is impregnated overnight at room temperature with $Ni(NO_3)_2{\cdot}6H_2O$ aqueous, dried at 110 °C for 6 h and calcined in air at 500 °C for 6 h, which is designated as the calcined (unreduced) catalyst sample.

The calcined catalyst sample contains Ni of 11 wt.% and Ce of 8 wt.%, which is determined by inductively coupled plasma-atomic emission spectroscopy (ICP-AES, Optima 2000DV, Perkin Elmer). The calcined catalyst can be auto-reduced in the PCR reactor[4], and hence it is not pre-reduced in this experiment.

The temperature distributions of catalyst bed (T_{CB}) and reactor wall (T_{RW}) for different temperatures of the heater, i.e., T_H of 1123, 1073, 1023, and 973 K are shown in figure S5, at a gas hourly space velocity (GHSV) of 6300 $mL{\cdot}g^{-1}{\cdot}h^{-1}$ and a total flow rate $\boldsymbol{F_t}$ of 4.3 SLM $CH_4/CO_2/O_2$ with molar ratio of 3/1/1. When the reaction occurs, T_{RW} increases gradually along the catalyst bed (figure S5), in contrast to the rather flat reference curve when no reaction occurs (T_{RW} no reaction, dull-red curve of figure S5).

The axial profiles of T_{CB} for various GHSV values are shown in figure S6.

Figure S7 indicates the axial distributions of T_{CB} and T_{RW} for $CH_4/CO_2/O_2$ molar ratios of 3/1/1 and 2.5/1/1. By tuning the $CH_4/CO_2/O_2$ molar ratio from 3/1/1 to 2.5/1/1, we need to change $\boldsymbol{F}_2$ when keeping the same plasma conditions (fixed $\boldsymbol{F}_1$). Therefore, two aspects need to be carefully considered, i.e., either to keep the same GHSV or the same amount of catalyst. When keeping the same GHSV, the amount of catalyst must be reduced. However, to keep consistency in the catalyst bed heating by the heater, the catalyst mid-bed position is fixed at the half-height of the heater in the experiments. Therefore, changing the amount of catalyst will cause a change in the distance between plasma and catalyst. The latter may have a significant influence on the reaction over the catalyst, because the active species and heat provided by the plasma greatly depend on the distance between plasma and catalyst bed.

Therefore, if the same amount of catalyst is preferred, we have to adapt the GHSV. The latter is 6300 or 5700 $mL{\cdot}g^{-1}{\cdot}h^{-1}$ for a $CH_4/CO_2/O_2$ molar ratio of 3/1/1 or 2.5/1/1, respectively. Indeed, a slight variation of around 10% in GHSV will have a minor effect on the reaction. Hence, we adopt

the same amount of catalyst in figure 8 with the specified GHSV of 6300 or 5700 mL·g^{-1}·h^{-1} for $CH_4/CO_2/O_2$ molar ratio of 3/1/1 or 2.5/1/1, respectively. Consequently, the GHSV of 5700 mL·g^{-1}·h^{-1} with $CH_4/CO_2/O_2$ molar ratio of 2.5/1/1 in figure 9 is adopted for the stability test in figure S8.

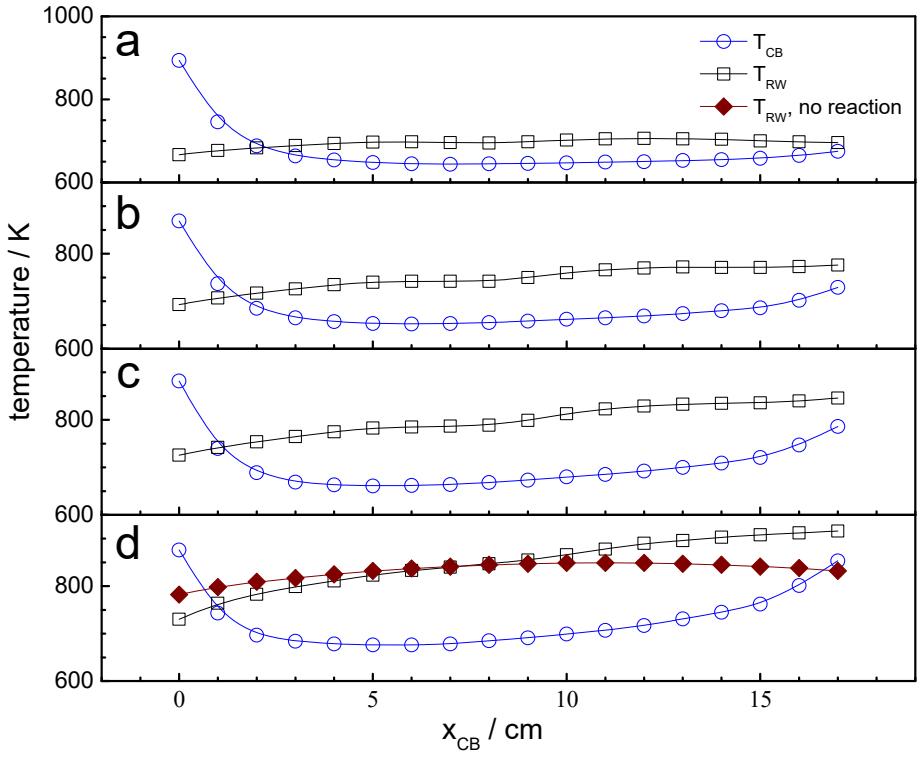

Figure S5. Axial profiles of T_{CB} and T_{RW} for different values of T_H, i.e., (a) 973 K, (b) 1023 K, (c) 1073 K and (d) 1123 K, at the same conditions as in figure 5 of the main paper. In (d), comparison is also made with T_{RW} without reaction, showing that T_{RW} with reaction is slightly lower than without in the first half of the post-plasma reactor, but it becomes larger in the second half, due to a small amount of unreacted CH_4.

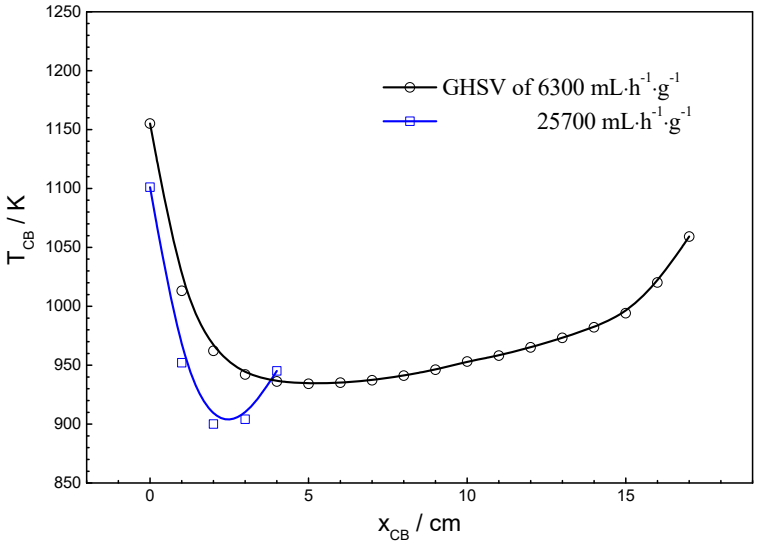

Figure S6. Axial profiles of T_{CB} for various GHSV values at T_H of 1073 K, at the same conditions as in figure 8 of the main paper.

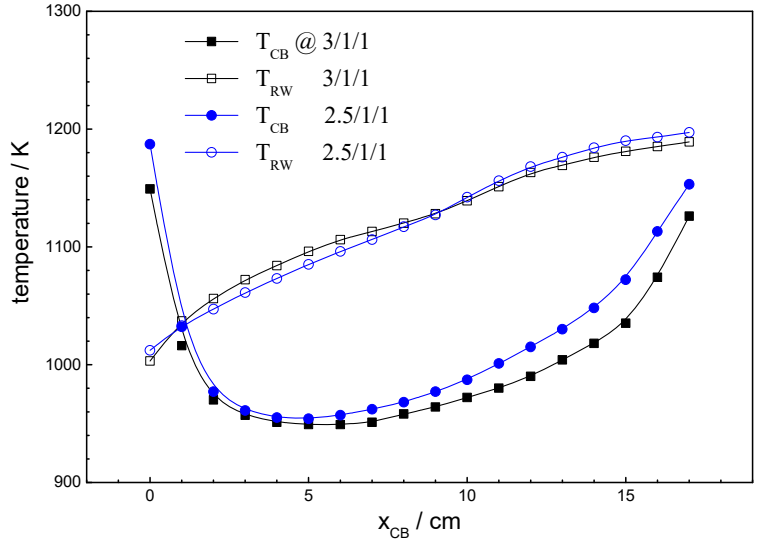

Figure S7. Effect of $CH_4/CO_2/O_2$ molar ratio on the axial profiles of T_{CB} and T_{RW} at T_H of 1123 K, at the same conditions as in figure 9 of the main paper.

S5 Stability test and carbon balance

Figure S8 shows the stability of the CH_4 and CO_2 conversion, syngas concentration and H_2/CO ratio, by plotting these values as a function of time-on-stream (TOS), i.e., operation time, at T_H of 1123 K, GHSV of 5700 mL·g^{-1}·h^{-1} and $CH_4/CO_2/O_2$ of 2.5/1/1 (0.9 SLM $\boldsymbol{F_2}$ and 3.9 SLM $\boldsymbol{F_t}$). After the 5-hour stability test, no coke formation on the catalyst sample is observed (figure S9). For the sake of comparison, we have also prepared a control catalyst sample by reducing a calcined (unreduced) sample in a gas stream of 5 vol.% H_2 in N_2 with a flow rate of 0.2 SLM at 1123 K for 1 h. While the calcined catalyst sample is light green, the used catalyst is black, just like the control catalyst sample (see figure S9), which may be ascribed to auto-reduction of NiO to Ni in the gas stream after the plasma[4].

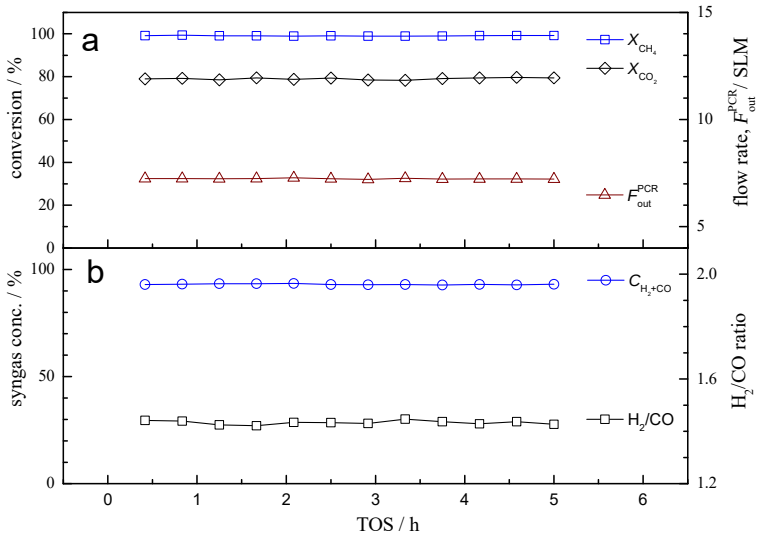

Figure S8. Stability test of (a) CH_4 and CO_2 conversion and flow rate of PCR outlet gas, and (b) syngas concentration and H_2/CO ratio, as a function of TOS at T_H of 1123 K, $CH_4/CO_2/O_2$ of 2.5/1/1 (0.9 SLM F_2 and 3.9 SLM F_t) and GHSV of 5700 mL·g^{-1}·h^{-1}.

Temperature programmed oxidation (TPO) is used to investigate coking of the used catalysts after reaction for 5-h TOS. The used catalysts of 41.0 g are mixed well and about half of them (20.1 g) are taken for TPO analysis. Prior to the TPO analysis, the sample is purged in N_2 flow at 573 K for 2.5 h and then cooled down to 473 K. Subsequently, 10% O_2/N_2 with a flow rate of 1 SLM is switched to replace the purge gas. It is heated from 473 to 1123 K with a ramp rate of 5

K/min, and then held at 1123 K for 4 h. The CO and CO_2 concentrations are detected by a CO_x analyzer (S710, Sick-Maihak, Germany). Figure S10 shows the temperature programmed oxidation (TPO) result of the used catalyst, to quantitatively determine coke formation, and Table S1 indicates whether coke is formed, as well as the carbon balance after the 5 hours stability test. The carbon balance is defined as the total carbon of the outlet gas divided by the total carbon of the inlet gas. The total carbon of the inlet gas is calculated according to the total flow rates of CH_4 and CO_2. No other carbonaceous species besides CH_4, CO_2 and CO are detected in the online GC analysis, hence the total carbon in the outlet gas is calculated based on the total flow rates of CH_4, CO_2 and CO.

Figure S9. Optical images of calcined (unreduced), control (reduced) and used (after the 5 hours stability tests) samples for $Ni/CeO_2/Al_2O_3$ catalysts.

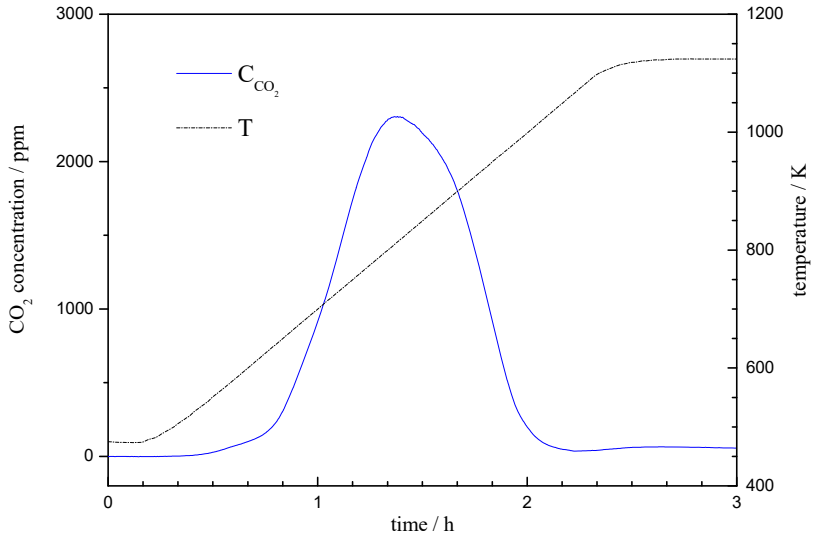

Figure S10. Analysis of temperature programmed oxidation on the used catalyst after the 5 hours stability test in figure S8.

Table S1. Coke formation and carbon balance after the 5 hours stability test in figure S8.

Carbon balance and coke formation	
total carbon of inlet gas / mol	40.2
total carbon of outlet gas / mol	39.7
carbon balance / %	98.8
coke / mol	0.032
ratio of coke to total carbon input / %	0.08

References

1. Zhu, B., Li, X. S., Shi, C., Liu, J. L., Zhao, T. L., Zhu, A. M. Pressurization effect on dry reforming of biogas in kilohertz spark-discharge plasma. *Int. J. Hydrogen Energy* 2012, **37:** 4945-4954.
2. Liu, J. L., Li, X. S., Zhu, X., Li, K., Shi, C., Zhu, A. M. Renewable and high-concentration syngas production from oxidative reforming of simulated biogas with low energy cost in a plasma shade. *Chem. Eng. J.* 2013, **234:** 240-246.
3. Li, K., Liu, J. L., Li, X. S., Zhu, X., Zhu, A. M. Post-plasma catalytic oxidative CO_2 reforming of methane over Ni-based catalysts. *Catal. Today* 2015, **256:** 96-101.
4. Li, K., Liu, J. L., Li, X. S., Zhu, X., Zhu, A. M. Warm plasma catalytic reforming of biogas in a heat-insulated reactor: Dramatic energy efficiency and catalyst auto-reduction. *Chem. Eng. J.* 2016, **288:** 671-679.
5. Zhao, T. L., Xu, Y., Song, Y. H., Li, X. S., Liu, J. L., Liu, J. B., Zhu, A. M. Determination of vibrational and rotational temperatures in a gliding arc discharge by using overlapped molecular emission spectra. *J. Phys. D: Appl. Phys.* 2013, **46:** 345201.
6. Kunze, H. J. *Introduction to Plasma Spectroscopy*, vol. 56. Springer, 2009.